# Accelerating Bayesian Sampling for Massive Black Hole Binaries with Prior Constraints from Conditional Variational Autoencoder

Hui Sun,[1, 2, 3, *] He Wang,[1, 2, 3, †] and Jibo He[1, 2, 3, 4, ‡]

[1]*University of Chinese Academy of Sciences (UCAS), Beijing 100049, China*
[2]*International Centre for Theoretical Physics Asia-Pacific, UCAS, Beijing 100190, China*
[3]*Taiji Laboratory for Gravitational Wave Universe (Beijing/Hangzhou), UCAS, Beijing 100190, China*
[4]*Hangzhou Institute for Advanced Study, UCAS, Hangzhou 310024, China*
(Dated: February 14, 2025)

We employ a Conditional Variational Autoencoder (CVAE) for parameter inference on massive black hole binaries (MBHBs), considering joint observations from a network of three space-based gravitational wave detectors. Our result demonstrates that the trained CVAE model can estimate the posterior distribution of source parameters in approximately 0.5 seconds, while the standard Bayesian sampling method, utilizing parallel computation across 16 CPU cores, takes an average of 22 hours across 25 MBHB signals. While the CVAE model achieves remarkable efficiency, its estimated distributions exhibit slight differences in shape compared to the standard Bayesian results, particularly showing lighter tails with broader widths. By using CVAE result to constrain the prior range for Bayesian sampling, we reduce the sampling time to 14.0% of the original runtime on average, while maintaining similar Bayesian result.

## I. INTRODUCTION

The first detection of gravitational waves (GW) [1] marked the beginning of a new era in astronomical and cosmological observations. Ground-based GW detectors have already identified numerous mergers of compact astrophysical objects. Space-based gravitational wave (GW) detectors, such as Taiji [2], LISA [3], and TianQin [4], are capable of observing GWs at significantly lower frequencies compared to ground-based detectors. Jointly considering multiple space-based gravitational wave detectors can enhance the detection capability and reliability of GW [5–7].

Massive black hole binary (MBHB) system is one of the primary sources of GW for space-based detectors. Investigating the detection [8] and parameter estimation [7, 9] of MBHB signals forms a fundamental aspect of this field. Bayesian inference, as a cornerstone of gravitational wave (GW) analysis, relies on Bayes' theorem to estimate the posterior probability of source parameters. In this context, the theorem is expressed as

$$p(\theta|d) = \frac{\mathcal{L}(d|\theta)\pi(\theta)}{\mathcal{Z}}, \qquad (1)$$

where $\theta$ denotes the GW parameters under consideration, and $d$ represents the strain data encompassing both detector noise and the detector response from GW signal. The term $\mathcal{Z} = \int \mathcal{L}(d|\theta)\pi(\theta)d\theta$ is the evidence, treated as a constant and often negligible. $\pi(\theta)$ signifies the prior distribution, and $\mathcal{L}(d|\theta)$ is the likelihood.

Sampling methods based on Bayesian inference, such as Markov Chain Monte Carlo (MCMC) [10–12] and

* sunhui22@mails.ucas.ac.cn
† hewang@ucas.ac.cn
‡ jibo.he@ucas.ac.cn

Nested Sampling (NS) [13], are widely implemented with high sampling precision, but they can be computationally demanding. Recent studies have explored the use of deep learning model for rapid posterior estimation of source parameters in ground-based GW detectors for stellar-mass black hole binaries, such as Conditional Variational Autoencoder (CVAE) [14] and nflows [15]. However, the current application of the deep learning model nflows for parameter estimation of MBHB systems tends to yield broader posterior distributions compared to the Bayesian inference method, with the discrepancy being approximately an order of magnitude [16].

To address discrepancies in the shapes of posterior distributions, while their widths remain generally consistent, between the parameter sampling results of deep learning models and those of standard Bayesian sampling methods for stellar-mass black hole binaries, a technique known as Neural Importance Sampling has been proposed. This method, as discussed in [17], reweights the samples generated by the deep learning model to correct inaccuracies in the estimated distributions. However, overly broad proposals can still result in low sample efficiency [17], limiting the effectiveness of this approach.

Building on the method that hierarchically reduces the parameter space for extreme-mass-ratio inspirals (EMRIs) using both physical and phenomenological waveforms, enabling precise parameter estimation [18], we extend this parameter space reduction approach to MBHB signals. Specifically, we extract boundary information from the CVAE-generated samples while ignoring the detailed shape of the distribution. This boundary information is then applied as a prior in Bayesian sampling, narrowing the prior range and accelerating the standard Bayesian sampling process. Other methods have also been proposed to accelerate the Bayesian sampling process for parameter estimation of GW signals, utilizing the properties of the GW. These include techniques such as Relative Binning [19, 20], Multibanding [21], and Re-

duced Order Quadrature [22]. These methods primarily achieve acceleration by modifying the likelihood rather than the prior.

This paper is organized as follows. In Sec. II, we briefly introduce the response mechanism of the space-based detectors network to GW, as well as the fundamental principle and sampling method of standard Bayesian inference and CVAE model for source parameter estimation. In Sec. III, we provide a detailed description of the training process and present the test result for an example GW signal. We constrain the prior range of source parameters using the testing result of CVAE, and perform Bayesian inference again with the narrowed prior range. We demonstrate a strong similarity between the Bayesian inference sampling results before and after narrowing the prior range, and also show the improvement in sampling speed achieved by narrowing the prior range. In Sec. IV, we present the conclusion of the paper.

## II. METHODOLOGY

### A. Space-Based Interferometers Network

We consider a network of three space-based GW detectors [23]: Taiji, TianQin, and LISA. Each detector moves along the Earth's orbit, spaced 20° apart from each other, with an orbital period of 1 year. Each space-based GW detector is equivalent to two independent two-arm detectors, denoted as the A and E channels of the space-based detector. Therefore, we will analyze a total of 6 independent channels in the detector network.

The response of each channel to the plus component $h_+$ and the cross component $h_\times$ of the GW is described as

$$s(t) = F_+ h_+(t) + F_\times h_\times(t), \tag{2}$$

where $F_+$ and $F_\times$ are the polarization response functions of the channel:

$$F_+ = D^{ij} e_{ij}^+, F_\times = D^{ij} e_{ij}^\times. \tag{3}$$

$D^{ij}$ is the detector tensor of the channel and $e_{ij}$ is the GW polarization tensor. The detector tensor $D^{ij}$ is related to the directions of the three arms of the space-based GW detector, and the detector tensors of the A and E channels are [9]

$$D_A^{ij} = \frac{1}{6} \left( u_1^i u_1^j - 2u_2^i u_2^j + u_3^i u_3^j \right), \tag{4}$$

$$D_E^{ij} = \frac{\sqrt{3}}{6} \left( u_1^i u_1^j - u_3^i u_3^j \right), \tag{5}$$

where $u_1^i, u_2^i, u_3^i$ represent the $i$-th components of the arm direction vectors for three arms. The GW polarization tensor $e_{ij}$ is relevant to the ecliptic latitude and ecliptic longitude of the GW source in the ecliptic coordinate system and the polarization angle of the GW. The detailed expression of the polarization response functions $F_+$ and $F_\times$ can be found in Ref. [24].

### B. Nested Sampling

In the context of Bayesian inference as expressed in Eq. (1), the likelihood function $\mathcal{L}(d|\theta)$ is defined as

$$\mathcal{L}(d|\theta) = \exp\left[ -\frac{1}{2} \langle d - s(\theta)|d - s(\theta) \rangle \right]. \tag{6}$$

Here, $s(\theta)$ represents the detector's response to the GW signal with parameters $\theta$. The inner product is defined as

$$\langle a|b \rangle = 4 \cdot \Re\left[ \int_0^\infty \frac{\tilde{a}(f)\tilde{b}^*(f)}{S_n(f)} df \right], \tag{7}$$

where $\tilde{a}(f)$ and $\tilde{b}(f)$ denote the Fourier transforms of $a(t)$ and $b(t)$, $\Re$ represents the extraction of the real part from the complex number, and $\tilde{b}^*(f)$ denotes the complex conjugate of $\tilde{b}(f)$. $S_n(f)$ represents the one-sided power spectral density. Its form is based on Ref. [25] for Taiji and TianQin, and on Ref. [26] for LISA.

Nested Sampling is a classic sampling method of Bayesian inference, first proposed by Skilling [13]. This method randomly generates sampling points of $\theta$ according to the prior $\pi(\theta)$ and iteratively selects $\theta_i$ in the i-th iteration with smaller prior volume $X$, which is defined as

$$X(\mathcal{L}) \equiv \int_{\mathcal{L}(\theta)>\mathcal{L}} \pi(\theta)d\theta. \tag{8}$$

The importance weighting $\hat{P}_i$ of $\theta_i$ is then calculated based on the prior volume $X_i$ estimated through statistical properties and the likelihood $\mathcal{L}_i$ computed using the likelihood function $\mathcal{L}(d|\theta)$, determined as

$$\hat{P}_i = \frac{\mathcal{L}_i(\hat{X}_{i-1} - \hat{X}_i)}{\sum_i \mathcal{L}_i(\hat{X}_{i-1} - \hat{X}_i)}. \tag{9}$$

The Nested Sampling procedure is as follows. Initially, $n_{\text{live}}$ samples are drawn from the prior $\pi(\theta)$ to act as live points for the first iteration. Subsequently, the sample with the lowest likelihood among the live points in the $i$-th iteration is removed as a dead point, with the prior volume of the dead point statistically set as $\hat{X}_i = \exp(-i/n_{\text{live}})$ [13]. This choice is based on the fact that the ratio of prior volumes between iterations, $t_i = X_i/X_{i-1}$, follows a Beta distribution, specifically denoted as $t_i \sim \beta(n_{\text{live}}, 1)$. A new live point is then sampled from a constrained prior that encloses the remaining live points, with the condition that its likelihood must exceed that of the most recently removed live point. This iterative process continues until the sampling precision meets the stopping criterion.

Several samplers based on the Nested Sampling framework are commonly developed, such as `PyMultiNest` [27–29], `dynesty` [30], `nestle` [31], and `PolyChord` [32]. In this work, we selected the `PyMultiNest` sampler, which is well parallelized, allowing us to perform multi-core CPU sampling. Specifically, we used 16 CPU cores for parallel sampling.
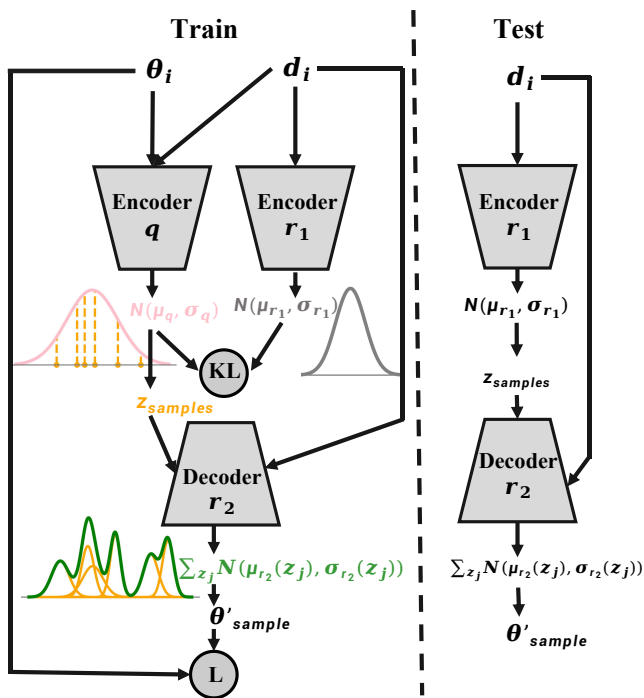
FIG. 1: The encoder-decoder configurations of CVAE used for training and testing processes. In the training process on the left side of the figure, both GW parameters $\theta_i$ and time-domain signal $d_i$ are input into the network. The encoders $q$ and $r_1$ generate the normal distribution $N(\mu_q, \sigma_q)$ and $N(\mu_{r_1}, \sigma_{r_1})$ in the latent space, and $z_{\text{samples}}$ are sampled from $N(\mu_q, \sigma_q)$. These samples are then input to the decoder $r_2$ along with $d_i$, resulting in a complex distribution approximating the Bayesian posterior probability $p(\theta|d_i)$. The KL divergence $D_{\text{KL}}$ is used to measure the similarity between the distributions $q_\phi(z|\theta_i, d_i)$ and $r_{\theta_1}(z|d_i)$. We use the sum of the error of the $\theta'$ sample relative to $\theta_i$ and the KL divergence as the loss during training. During testing on the right side of the figure, by sequentially inputting $d_i$ into encoder $r_1$ and decoder $r_2$, we can obtain samples of $\theta'$ to estimate the parameters posterior of $d_i$.

## C. CVAE model

In this paper, we utilize the Conditional Variational Autoencoder (CVAE) model [33], comprising two encoders denoted as $r_1$ and $q$, and a decoder denoted as $r_2$. The structure of CVAE is illustrated in Fig. 1. During the training process depicted in Fig. 1, the strain data $d_i$ and the corresponding GW source parameters $\theta_i$ from the $i$-th instance of the dataset are fed into the encoder $q$. Subsequently, the encoder $q$ generates the mean $\mu_q$ and standard deviation $\sigma_q$ to construct a normal distribution $N(\mu_q, \sigma_q)$ for the latent variable $z$. Sampling is then performed from the distribution $N(\mu_q, \sigma_q)$ to generate $z_{\text{samples}}$.

Each $z_j \in z_{\text{samples}}$ is input to the decoder $r_2$ along with $d_i$, resulting in the mean $\mu_{r_2}(z_j)$ and standard deviation $\sigma_{r_2}(z_j)$ to construct a normal distribution $N(\mu_{r_2}(z_j), \sigma_{r_2}(z_j))$ of $\theta'$. By combining all normal distributions corresponding to $z_{\text{samples}}$, a complex distribution can be constructed to approximate the Bayesian posterior distribution $p(\theta|d_i)$. However, this process requires the input to include $\theta_i$, which is not available when testing $d_i$ with unknown $\theta_i$.

To address this issue, the model introduces the encoder $r_1$. By inputting only $d_i$ into encoder $r_1$ to obtain the normal distribution $N(\mu_{r_1}, \sigma_{r_1})$ and training the model to minimize the discrepancy between $N(\mu_{r_1}, \sigma_{r_1})$ and $N(\mu_q, \sigma_q)$, encoder $r_1$ can be utilized during testing to generate the distribution of the latent variable $z$ instead of encoder $q$, as demonstrated in the testing process depicted in Fig.1.

The discrepancy between the distribution $r_{\rho_1}(z|d_i) \equiv N(\mu_{r_1}, \sigma_{r_1})$ and the distribution $q_\phi(z|\theta_i, d_i) \equiv N(\mu_q, \sigma_q)$ can be assessed using the Kullback-Leibler (KL) divergence $D_{\text{KL}}$ between the two distributions, defined as

$$D_{\text{KL}}\left(q_\phi(z|\theta_i, d_i)||r_{\rho_1}(z|d_i)\right) \qquad (10)$$
$$\equiv \int \mathrm{d}z \ q_\phi(z|\theta_i, d_i) log\left[\frac{q_\phi(z|\theta_i, d_i)}{r_{\rho_1}(z|d_i)}\right].$$

The discrepancy between the true posterior $p(\theta|d_i)$ and the distribution $r_{\rho_2}(\theta'|z, d_i) = \frac{1}{n}\sum_j^n N(\mu_{r_2}(z_j), \sigma_{r_2}(z_j))$ estimated by the model can be quantified using the reconstruction loss $-E_{q_\phi(z|\theta_i, d_i)}[\log r_{\rho_2}(\theta_i|z, d_i)]$. Here, the variable $n$ denotes the total number of $z_{\text{samples}}$.

In the context of the CVAE model, it can be demonstrated that the sum of the KL divergence loss and the reconstruction loss serves as an upper bound on the true loss of the model. A detailed proof of this statement can be found in Ref. [14, 34]. When training the model, we combine these two losses to encapsulate the overall loss of the model.

## III. TRAINING AND PRIOR NARROWING

### A. Data Generation and Training Model

The training set comprises $6 \times 10^5$ instances of training data, with each instance containing both strain data from 6 channels across 3 detectors as features and waveform parameters as labels. Strain data from each of the 6 channels is a time series with a data length of 16384, sampled at a frequency of 1/16 Hz, resulting in a duration of approximately 3 days for each time series. The plus component $h_+$ and the cross component $h_\times$ of the GW are constructed using the dominant $(2, 2)$ mode generated by the IMRPhenomPv3 [35] approximation model. Each strain data is obtained by superimposing a response data from a MBHB GW waveform signal generated using PyCBC [36] and a random noise produced by the noise power spectral
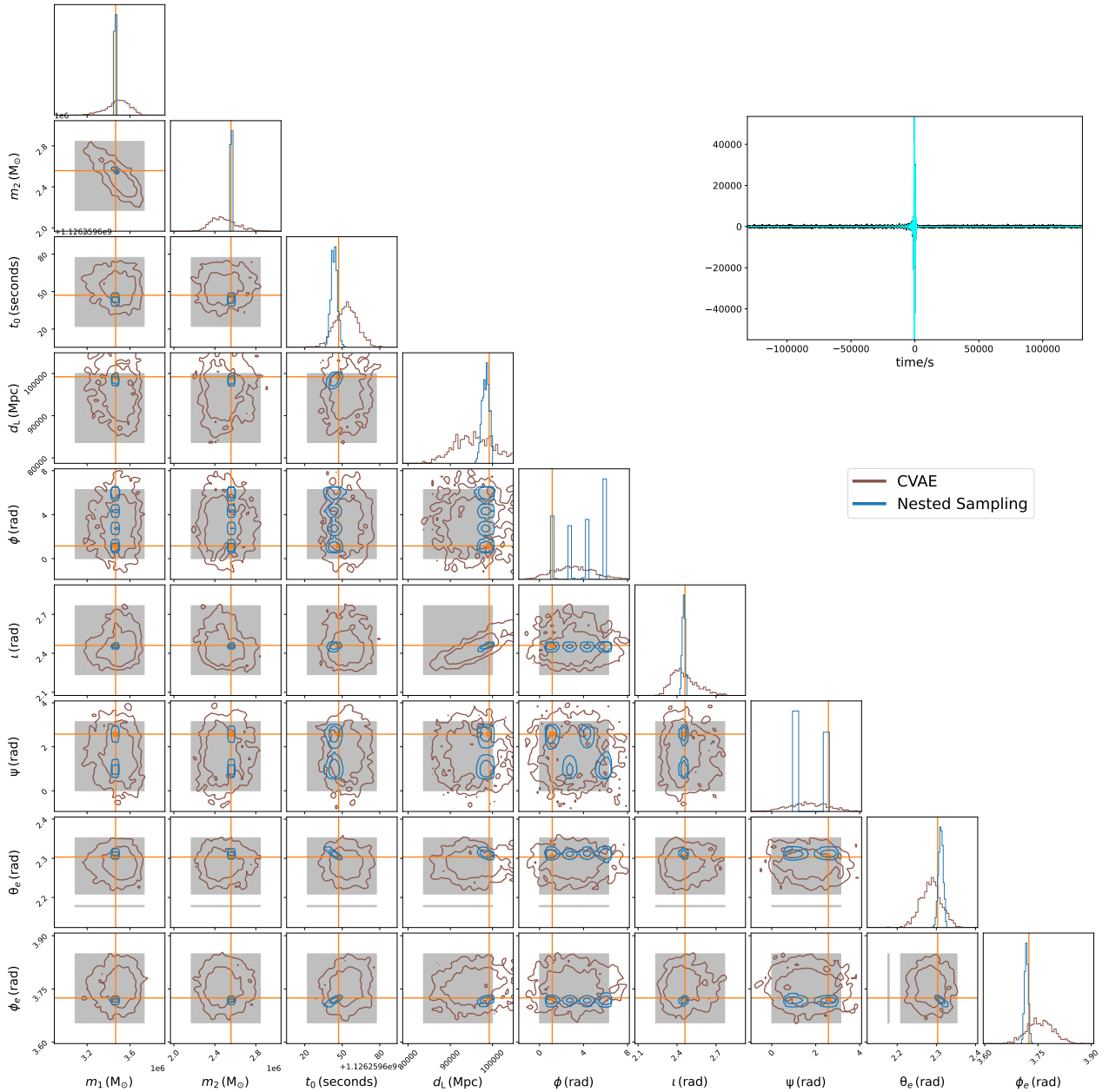
FIG. 2: The distribution of source parameters obtained using the CVAE method (brown) and standard Bayesian sampling method (blue). The result contours of each method correspond to the 68% and 95% confidence levels. The histograms on the diagonal represent the posterior probability distribution for each parameter. The orange solid lines on the contour plot represent the true values of the parameters. We highlight in gray the constrained prior range derived from the CVAE results and the initial full prior range. In the upper right corner, there are a whitened noisy signal (black) and a whitened noiseless signal (light blue) from the A-channel of Taiji.

density (PSD) of each detector. The strain data is further whitened by dividing it by the PSD of each detector to produce a dataset suitable for training. The test set comprises 25 instances of test data, with the same instance structure as the one of training set. Additionally, the test set will be used as the validation set.

The gravitational wave source parameters $\theta$ consist of 9 parameters, including the two black hole masses $m_1$ and $m_2$ of the MBHB, the GPS time $t_0$ at the merger of the MBHB, the luminosity distance $d_L$ of the MBHB to the detector, the phase $\phi$ at the merger of the MBHB, the inclination angle $\iota$, the polarization angle $\psi$, the ecliptic latitude $\theta_e$, and the ecliptic longitude $\phi_e$ of the MBHB source in the ecliptic coordinate system. The default
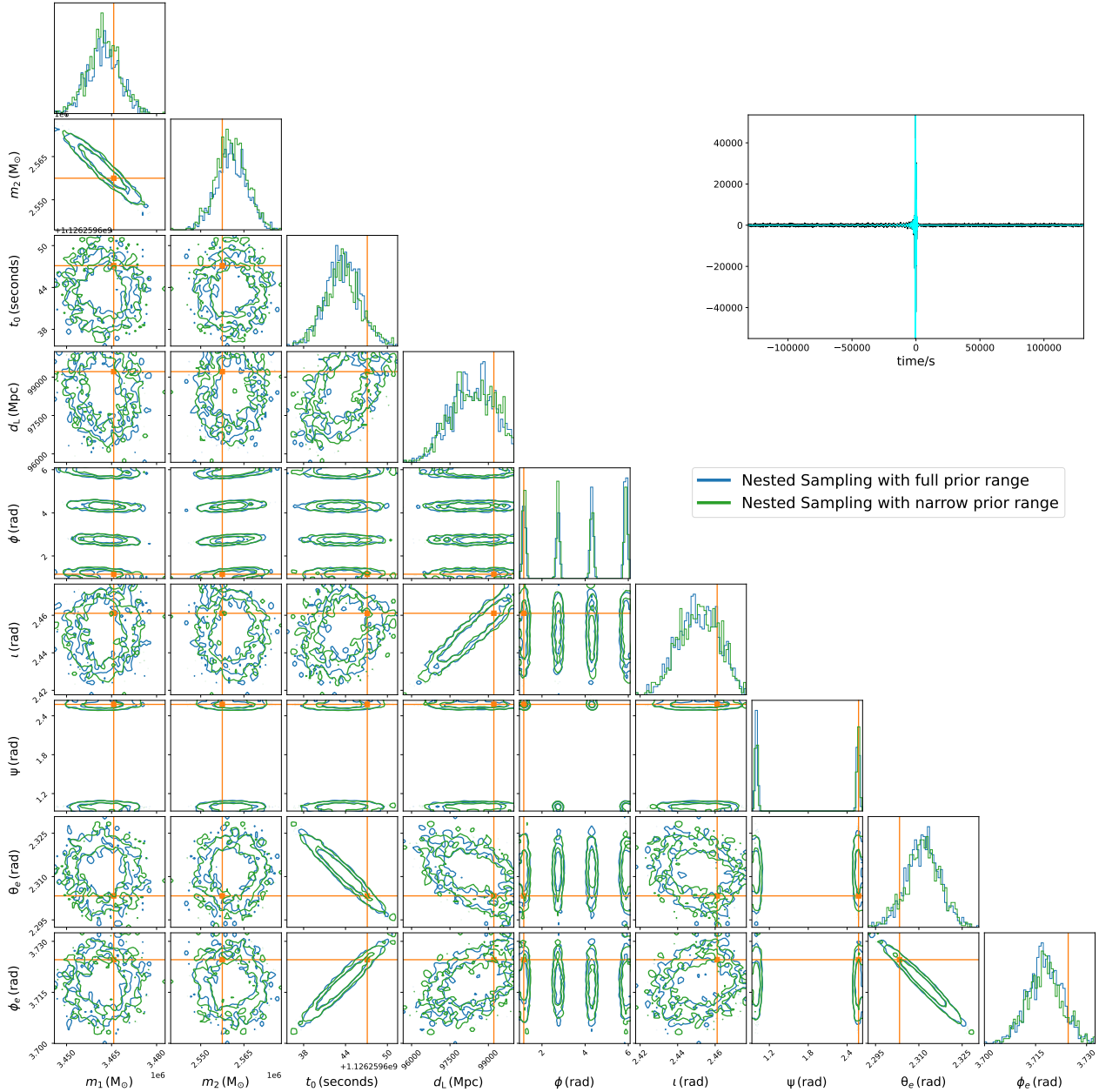
FIG. 3: The distribution of source parameters obtained using the standard Bayesian sampling method under the initial full prior (blue) and the narrowed prior (green). The result contours of each method correspond to the 68% and 95% confidence levels. The orange solid lines are the true parameter values of the injected instance.

priors of these 9 parameters are specified as shown in Table I.

During the training process, we adopt a strategy of decreasing the learning rate as the number of iteration increases. Setting a relatively large learning rate initially can prevent the model from getting stuck in local minima or saddle points. As the number of training iterations increases, decreasing the learning rate continuously can prevent the model from jumping back and forth between different low points of the loss function, helping the model

find the minimum of the loss function. During model training, we employ the InverseTimeDecay function as the learning rate schedule, defined as $r = r_0/(1 + i/10^5)$. Here, $r_0$ denotes the initial learning rate, which is fixed at $1 \times 10^{-4}$, and $i$ represents the training iteration. We train the model until the total loss ceased to decrease significantly with further iterations. This process takes two days on an A800 GPU, utilizing 68 GB of GPU memory during training and completing $2 \times 10^5$ iterations.

The parameter estimation result for one test instance

TABLE I: Default MBHB priors settings. The distribution of $\cos(\iota)$ and $\cos(\theta_e)$ is uniform to guarantee isotropy in space. Other parameters are set to be uniform in their specific ranges. And $t_r$ is the reference GPS time, set to 1126259643.

| Variable | Description | Prior | Minimum | Maximum | Units |
|----------|-------------|-------|---------|---------|-------|
| $m_1$ | mass 1 | Uniform | $10^5$ | $10^7$ | $M_\odot$ |
| $m_2$ | mass 2 | Uniform | $10^5$ | $10^7$ | $M_\odot$ |
| $t_0$ | coalescence time | Uniform | $t_r - 256$ | $t_r + 256$ | $s$ |
| $d_L$ | luminosity distance | Uniform | $10^3$ | $10^5$ | Mpc |
| $\phi$ | coalescence phase | Uniform | 0 | $2\pi$ | rad |
| $\iota$ | inclination angle | Sine | 0 | $\pi$ | rad |
| $\psi$ | polarization angle | Uniform | 0 | $\pi$ | rad |
| $\theta_e$ | ecliptic latitude | Sine | 0 | $\pi$ | rad |
| $\phi_e$ | ecliptic longitude | Uniform | 0 | $2\pi$ | rad |

with signal-to-noise ratio (SNR) of 501.2 is shown in Fig. 2, where the brown contour plot represents the estimation result of the CVAE model, and the blue contour plot represents the result obtained using the standard Bayesian sampling method.

### B. Reducing Prior Range

In the Bayesian framework, where the prior $\pi(\theta)$ is non-zero and the likelihood $\mathcal{L}(d|\theta)$ is zero, the posterior $p(\theta|d)$ will be zero. If we set the prior to zero in these regions, the posterior remains zero. Therefore, it is reasonable to set the prior to zero in the region where the prior is non-zero but the likelihood is very small. This approach can effectively reduce the scope of the prior without substantially affecting the overall posterior distribution and is largely equivalent to bypassing the generation of low-weight sampling points during the initial stages of Nested Sampling.

The trained CVAE model estimates the parameters of a single instance in approximately 0.5 seconds, while the Nested Sampling method, leveraging parallel computation across 16 CPU cores using the PyMultiNest sampler, requires an average of 22.0 hours for 25 test instances in the Bilby framework [37, 38]. Although the trained model has relatively weaker parameter constraint capabilities, its significant computational speed advantage over Nested Sampling makes it suitable for preprocessing the prior for Nested Sampling. By narrowing the prior range, the initial sampling space is reduced, thereby accelerating the sampling process. Specifically, we determine the prior range by selecting the contiguous intervals corresponding to the cumulative probabilities from 0.135% to 99.865% of each source parameter's distribution estimated by the CVAE model, as indicated by the gray-shaded regions in Fig. 2. For regions outside the full prior space identified by the CVAE, primarily in the parameters $\phi$ and $\psi$, we exclude them from consideration. For unexpected secondary intervals, such as the small segment appearing on the left side of the $\theta_e$ parameter in the figure, we automatically split the

prior into corresponding sub-intervals. These unintended multi-segmented intervals would not impose any significant additional computational burden on the subsequent Nested Sampling process.

Figure 3 presents the results of the Nested Sampling method with and without the use of the trained CVAE model to narrow the prior region. The comparison reveals that the accuracy and precision of the two distributions are nearly identical, indicating that the CVAE-reduced prior does not significantly impact the posterior distribution of the instance. After preprocessing with the CVAE model, the runtime of Nested Sampling for the GW instance shown in Figs. 2 and 3 is reduced from 47.5h to 3.5h under parallel computation, which is 7.4% of the time required for a full sampling run. Across the 25 instances in the test set, the runtime is reduced to 14.0% of the original sampling time on average. These results highlight the effectiveness of using deep learning as a preprocessing step for parameter estimation.

We use symmetric KL divergence to evaluate the similarity of the Nested Sampling results after and before narrowing the prior across 25 instances, as shown in Fig. 4, labeled as "narrow NS vs. full NS". A symmetric KL divergence value of 0 indicates perfect similarity between two distributions. However, due to inherent sampling uncertainty, the KL divergence between two runs of the same instance is typically slightly greater than 0. To quantify this uncertainty, we perform two independent runs using the full prior, and calculate the corresponding KL divergence across 25 instances, labeled as "full NS vs. full NS". Furthermore, we compare the parameter posterior estimated by the CVAE model with the Nested Sampling posterior obtained using the full prior. This comparison is labeled as "CVAE vs. full NS".

By comparing the symmetric KL divergence values of "CVAE vs. full NS" and "full NS vs. full NS" we find that the symmetric KL divergence of "CVAE vs. full NS" is larger than that of "full NS vs. full NS" indicating that the estimation accuracy of the CVAE model is somewhat inferior to that of the standard sampling method. Additionally, by comparing the symmetric KL divergence values of "narrow NS vs. full
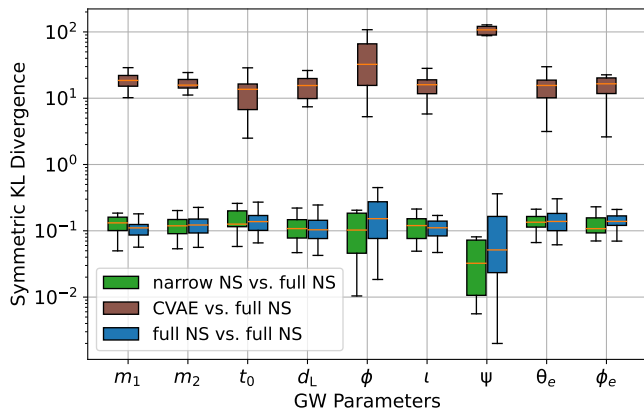
FIG. 4: Boxplot illustrating the symmetric KL divergence distribution of 25 GW instances across different methods. The box represents the interquartile range, which spans from the 25th percentile to the 75th percentile. The orange line inside the box represents the median. The whiskers extend to the most extreme data points within 1.5 times the the interquartile range from the box. We present a boxplot (green) showing the KL divergence results between Nested Sampling runs with CVAE-reduced prior (narrow NS) and Nested Sampling runs with complete prior (full NS) for 25 GW instances. This is compared with the boxplots of CVAE vs. full NS (brown) and full NS vs. full NS from two repeated runs of Nested Sampling with complete priors (blue).

NS" and "full NS vs. full NS" we find that the two have a similar magnitude, suggesting that narrowing the prior has minimal impact on the Nested Sampling results.

## IV. CONCLUSIONS

In this study, we employ the CVAE model to estimate the posterior of source parameters for unknown MBHB time-domain signals through neural network training. The variational nature of CVAE enables the generation of complex parameter distributions. The CVAE model is trained for 2 days on an A800 GPU, using $6\times10^5$ training instances and occupying approximately 68 GB of GPU memory during training. Following training, the model is evaluated on a test set comprising 25 instances to obtain their source parameter distributions. Standard posterior sampling for GW parameters is computationally intensive, typically requiring significant time and resources. In contrast, the trained CVAE model demonstrates superior efficiency, with an average sampling time of ap-

proximately 0.5 seconds per instance, compared to the standard posterior sampling method, which takes 22.0 hours on average across test set when executed through parallel processing on a CPU with 16 cores.

However, compared to the standard posterior sampling method, the CVAE results exhibit a certain degree of light-tailed behavior, with the distribution widths spanning several orders of magnitude relative to the standard Bayesian results. Given that CVAE processes MBHB signals in less than 1 second, we propose that for cases requiring higher precision in parameter estimation, CVAE can be employed to preprocess gravitational wave time-domain signals to narrow down the prior range of the standard Bayesian sampling method. By selecting parameter intervals corresponding to cumulative probabilities ranging from 0.135% to 99.865% based on CVAE estimation results, a more restricted prior range can be established to accelerate the standard posterior sampling process.

In our experiments, the standard posterior sampling time for 25 test instances is reduced to an average of just 14.0% of the original runtime required for sampling with the full prior. Furthermore, by evaluating the similarity between the sampling results before and after narrowing down the prior range, we demonstrate that the level of agreement is comparable to the symmetric KL divergence observed in the two independent full Nested Sampling runs.

This method can also be applied to other gravitational wave sources with high signal-to-noise ratios, where differences remain in the precision of parameter estimation between the deep learning method and the standard Bayesian sampling method.

Added-in-proof. While finalizing the draft, we become aware of a recently submitted related study [39] that also employs CVAE-generated priors for Bayesian sampling. Their work focuses on lensed gravitational wave signals from stellar-mass black hole binaries, specifically targeting two lensing-related parameters.

[1] B. P. Abbott, R. Abbott, T. Abbott, M. Abernathy, F. Acernese, K. Ackley, C. Adams, T. Adams, P. Addesso, R. X. Adhikari, *et al.*, Observation of gravitational waves from a binary black hole merger, Phys. Rev. Lett. **116**, 061102 (2016).
[2] W.-R. Hu and Y.-L. Wu, The taiji program in space for

gravitational wave physics and the nature of gravity, National Science Review **4**, 685 (2017).

[3] P. Amaro-Seoane, H. Audley, S. Babak, J. Baker, E. Barausse, P. Bender, E. Berti, P. Binetruy, M. Born, D. Bortoluzzi, *et al.*, Laser interferometer space antenna (2017), arXiv:1702.00786 [astro-ph.IM].

[4] J. Luo, L.-S. Chen, H.-Z. Duan, Y.-G. Gong, S. Hu, J. Ji, Q. Liu, J. Mei, V. Milyukov, M. Sazhin, *et al.*, Tianqin: a space-borne gravitational wave detector, Classical and Quantum Gravity **33**, 035010 (2016).

[5] Y. Gong, J. Luo, and B. Wang, Concepts and status of chinese space gravitational wave detection projects, Nature Astronomy **5**, 881 (2021).

[6] C. Zhang, Y. Gong, H. Liu, B. Wang, and C. Zhang, Sky localization of space-based gravitational wave detectors, Phys. Rev. D **103**, 103013 (2021).

[7] Q. Hu, M. Li, R. Niu, and W. Zhao, Joint observations of space-based gravitational-wave detectors: Source localization and implications for parity-violating gravity, Phys. Rev. D **103**, 064057 (2021).

[8] I. W. Harry, S. Fairhurst, and B. S. Sathyaprakash, A hierarchical search for gravitational waves from supermassive black hole binary mergers, Classical and Quantum Gravity **25**, 184027 (2008).

[9] S. Marsat, J. G. Baker, and T. D. Canton, Exploring the bayesian parameter estimation of binary black holes with lisa, Phys. Rev. D **103**, 083011 (2021).

[10] W. K. Hastings, Monte carlo sampling methods using markov chains and their applications, Biometrika **57**, 97 (1970).

[11] N. Christensen and R. Meyer, Using markov chain monte carlo methods for estimating parameters with gravitational radiation data, Phys. Rev. D **64**, 022001 (2001).

[12] V. Raymond, M. V. van der Sluys, I. Mandel, V. Kalogera, C. Röver, and N. Christensen, The effects of ligo detector noise on a 15-dimensional markov-chain monte carlo analysis of gravitational-wave signals, Classical and Quantum Gravity **27**, 114009 (2010).

[13] J. Skilling, Nested sampling for general Bayesian computation, Bayesian Analysis **1**, 833 (2006).

[14] H. Gabbard, C. Messenger, I. S. Heng, F. Tonolini, and R. Murray-Smith, Bayesian parameter estimation using conditional variational autoencoders for gravitational-wave astronomy, Nature Physics **18**, 112 (2022).

[15] S. R. Green and J. Gair, Complete parameter inference for gw150914 using deep learning, Machine Learning: Science and Technology **2**, 03LT01 (2021).

[16] M. Du, B. Liang, H. Wang, P. Xu, Z. Luo, and Y. Wu, Advancing space-based gravitational wave astronomy: Rapid parameter estimation via normalizing flows, Sci. China Phys. Mech. Astron. **67**, 230412 (2024), arXiv:2308.05510 [astro-ph.IM].

[17] M. Dax, S. R. Green, J. Gair, M. Pürrer, J. Wildberger, J. H. Macke, A. Buonanno, and B. Schölkopf, Neural importance sampling for rapid and reliable gravitational-wave inference, Phys. Rev. Lett. **130**, 171403 (2023).

[18] C.-Q. Ye, H.-M. Fan, A. Torres-Orjuela, J.-d. Zhang, and Y.-M. Hu, Identification of gravitational waves from extreme-mass-ratio inspirals, Phys. Rev. D **109**, 124034 (2024).

[19] B. Zackay, L. Dai, and T. Venumadhav, Relative binning and fast likelihood evaluation for gravitational wave parameter estimation (2018), arXiv:1806.08792 [astro-ph.IM].

[20] N. Leslie, L. Dai, and G. Pratten, Mode-by-mode relative binning: Fast likelihood estimation for gravitational waveforms with spin-orbit precession and multiple harmonics, Phys. Rev. D **104**, 123030 (2021).

[21] S. Vinciguerra, J. Veitch, and I. Mandel, Accelerating gravitational wave parameter estimation with multi-band template interpolation, Classical and Quantum Gravity **34**, 115006 (2017).

[22] P. Canizares, S. E. Field, J. Gair, V. Raymond, R. Smith, and M. Tiglio, Accelerated gravitational wave parameter estimation with reduced order modeling, Phys. Rev. Lett. **114**, 071104 (2015).

[23] R.-G. Cai, Z.-K. Guo, B. Hu, C. Liu, Y. Lu, W.-T. Ni, W.-H. Ruan, N. Seto, G. Wang, and Y.-L. Wu, On networks of space-based gravitational-wave detectors, Fundamental Research **4**, 1072 (2024).

[24] D. Liang, Y. Gong, A. J. Weinstein, C. Zhang, and C. Zhang, Frequency response of space-based interferometric gravitational-wave detectors, Phys. Rev. D **99**, 104027 (2019).

[25] H. Liu, C. Zhang, Y. Gong, B. Wang, and A. Wang, Exploring nonsingular black holes in gravitational perturbations, Phys. Rev. D **102**, 124011 (2020).

[26] R. Niu, X. Zhang, T. Liu, J. Yu, B. Wang, and W. Zhao, Constraining screened modified gravity with spaceborne gravitational-wave detectors, The Astrophysical Journal **890**, 163 (2020).

[27] J. Buchner, A. Georgakakis, K. Nandra, L. Hsu, C. Rangel, M. Brightman, A. Merloni, M. Salvato, J. Donley, and D. Kocevski, X-ray spectral modelling of the agn obscuring region in the cdfs: Bayesian model selection and catalogue, Astronomy & Astrophysics **564**, A125 (2014).

[28] F. Feroz and M. P. Hobson, Multimodal nested sampling: an efficient and robust alternative to markov chain monte carlo methods for astronomical data analyses, Monthly Notices of the Royal Astronomical Society **384**, 449 (2008).

[29] F. Feroz, M. P. Hobson, and M. Bridges, Multinest: an efficient and robust bayesian inference tool for cosmology and particle physics, Monthly Notices of the Royal Astronomical Society **398**, 1601 (2009).

[30] J. S. Speagle, dynesty: a dynamic nested sampling package for estimating bayesian posteriors and evidences, Monthly Notices of the Royal Astronomical Society **493**, 3132 (2020).

[31] K. Barbary, nestle: Pure python, mit-licensed implementation of nested sampling algorithms for evaluating bayesian evidence, https://github.com/kbarbary/nestle.

[32] W. J. Handley, M. P. Hobson, and A. N. Lasenby, polychord: next-generation nested sampling, Monthly Notices of the Royal Astronomical Society **453**, 4384 (2015).

[33] K. Sohn, H. Lee, and X. Yan, Learning structured output representation using deep conditional generative models, in *Advances in Neural Information Processing Systems*, Vol. 28, edited by C. Cortes, N. Lawrence, D. Lee, M. Sugiyama, and R. Garnett (Curran Associates, Inc., 2015).

[34] F. Tonolini, J. Radford, A. Turpin, D. Faccio, and R. Murray-Smith, Variational inference for computational imaging inverse problems, Journal of Machine Learning Research **21**, 1 (2020).

[35] S. Khan, K. Chatziioannou, M. Hannam, and F. Ohme,

Phenomenological model for the gravitational-wave signal from precessing binary black holes with two-spin effects, Phys. Rev. D **100**, 024059 (2019).

[36] C. M. Biwer, C. D. Capano, S. De, M. Cabero, D. A. Brown, A. H. Nitz, and V. Raymond, Pycbc inference: A python-based parameter estimation toolkit for compact binary coalescence signals, Publications of the Astronomical Society of the Pacific **131**, 024503 (2019).

[37] G. Ashton, M. Hübner, P. D. Lasky, C. Talbot, K. Ackley, S. Biscoveanu, Q. Chu, A. Divakarla, P. J. Easter, B. Goncharov, *et al.*, Bilby: A user-friendly bayesian inference library for gravitational-wave astronomy, The As-

trophysical Journal Supplement Series **241**, 27 (2019).

[38] I. M. Romero-Shaw, C. Talbot, S. Biscoveanu, V. D'emilio, G. Ashton, C. Berry, S. Coughlin, S. Galaudage, C. Hoy, M. Hübner, *et al.*, Bayesian inference for compact binary coalescences with bilby: validation and application to the first ligo–virgo gravitational-wave transient catalogue, Monthly Notices of the Royal Astronomical Society **499**, 3295 (2020).

[39] R. B. Nerin, O. Bulashenko, O. G. Freitas, and J. A. Font, Parameter estimation of microlensed gravitational waves with conditional variational autoencoders (2024), arXiv:2412.00566 [gr-qc].